Digital Object Identifier 10.1109/ECCE47101.2021.9595694

2021 IEEE Energy Conversion Congress and Exposition (ECCE)

Impact of Partial Power Processing Dual-Active Bridge Converter on Li-ion Battery Storage Systems

Hamzeh Beiranvand

Felix Hoffmann

Frederik Hahn

Marco Liserre

Suggested Citation

H. Beiranvand, F. Hoffmann, F. Hahn and M. Liserre, "Impact of Partial Power Processing Dual-Active Bridge Converter on Li-ion Battery Storage Systems," 2021 IEEE Energy Conversion Congress and Exposition (ECCE), 2021.

Impact of Partial Power Processing Dual-Active Bridge Converter on Li-ion Battery Storage Systems

Hamzeh Beiranvand
Chair of Power Electronics
Kiel University
Kiel, Germany
hab@tf.uni-kiel.de

Felix Hoffmann
Chair of Power Electronics
Kiel University
Kiel, Germany
fho@tf.uni-kiel.de

Frederik Hahn
Chair of Power Electronics
Kiel University
Kiel, Germany
frha@tf.uni-kiel.de

Marco Liserre
Chair of Power Electronics
Kiel University
Kiel, Germany
ml@tf.uni-kiel.de

***Abstract*—Partial Power Processing converters (PPPCs) provide economical and highly efficient solutions to integrate battery energy storages systems (BSSs) into DC grids. Beside these significant advantages, direct connection of the batteries by PPPCs to DC grids imposes challenges on the operation of batteries which need more evaluation. DC grid imperfections such as harmonics and faults may directly propagate into BSS and result in battery capacity fade acceleration and/or battery failure. In this paper, low voltage (LV) grid imperfection impacts are compared for conventional dual-active bridge (DAB) and Partial Power Processing DAB (PPP-DAB) converters. Both theoretical and experimental studies are carried out. The obtained results show that PPP-DAB exposes the BSS to high amount of current harmonics and safety issues.**

***Index Terms*—Partial Power Processing, Dual-Active Bridge (DAB) Converter, Lithium Ion Battery, Harmonics, External Short-Circuits, Transient Over-Voltages**

I. Introduction

By mass-production of Li-ion (Lithium-ion) batteries and the reduced costs, their application to different battery energy storage systems (BSSs) is rapidly growing [1]. Safe operation of the battery is a prerequisite to prevent reduction/decomposition of electrolyte material as well mechanical stresses from volume changes [2], [3]. External stresses on batteries are mainly from the environment and the interconnecting power electronic converters. Power electronics converters are mainly used to control the charging/discharging of Li-ion batteries and therefore they can strongly influence the electrochemical and mechanical degradation of this kind of BSSs.

Normally, full power processing converters (FPPCs) are used for BSS integration. In some applications such as electric vehicle charging stations, galvanic isolation is a safety requirement and isolated converters are mandatory to integrate BSSs to the grid [4]–[6]. However, in some of the stationary BSSs applications, non-isolated integration to the low voltage (LV) DC grid is possible which enhances the flexibility of the power converter design and configuration [7]. The well-known synchronous DC-DC converter is usually used in non-isolated BSS applications [8]. In this regard, to reduce the converter rating and to further improve the efficiency, the concept of PPPC topologies has been proposed, recently [9]. This concept aims to arrange an energy source as a series or a parallel element with the load/grid, and allows that only a fraction of the full power is transferred through the converter. The direct power path between the source and the load port affects the electrical characteristics of the converter and as a consequence also the battery storage. The resulting issues with PPPC has not been analyzed yet from the battery perspective.

Overcharge and overdischarge faults which might lead to thermal runaway do not originate from the power converter. They originate from the malfunctioning of the BMS functions in balancing the voltage and state of charge (SoC) of individual cells [10]–[12]. Faults such as internal short-circuits are unlikely but possibly severe consequences [13]–[15]. Mechanical issues such as penetration of a sharp nail and environment conditions can also result in internal short-circuits and finally the explosion of the BSSs [16]–[18]. These faults can occur independent from the impacts of the connected grid and power electronics. However, power quality issues, external short-circuits (SCs) and transient over-voltages (TOVs) directly root from the power converter or propagate through the power converter to Li-ion batteries.

Voltage and current harmonics are power quality issues with a permanent nature. The presence of harmonics can put stress on the performance of electrical components such as batteries if they have sufficiently large magnitudes. Current ripples increase the charging time, the average effective charging current and extra temperature rise of the Li-ion battery depending on the ripple waveform [19]. Lower frequency harmonics have been proven to have a higher effect on the Li-ion battery lifetime degradation [20]. However, also high frequency harmonics should be limited for utilizing maximum capacity of the BSS without extra heat generation and other chemical effects. TOVs and SCs are among the most usual ways of BSS failure [21]. SCs cause high rate of current flowing inside the cell and may excite exothermic reactions and thermal runaway. TOVs, such as lightening surges, occur at high frequencies and have minimal effect on the electrochemical reactions while TOVs might destroy the separator if they exceed the breakdown level.

The target of the paper is to evaluate the impacts of PPPC on the BSS from power quality and safety aspects. One Li-ion

Funded by the European Union - European Regional Development Fund (EFRE), the German Federal Government and the State of Schleswig-Holstein.

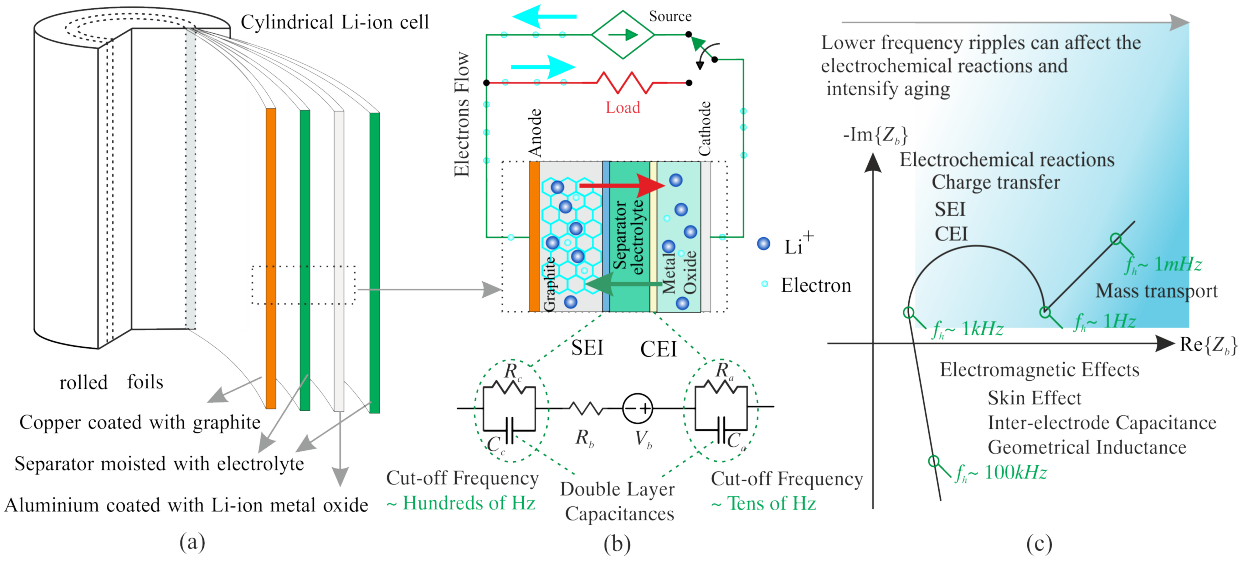

Fig. 1. Li-ion battery cell properties: (a) Lithium-ion battery cell with cylindrical geometry, (b) electrochemical process in the anode-electrolyte-cathode interface and the equivalent circuit model, and (c) impedance spectroscopy of the lithium-ion battery showing its frequency domain behavior.

based BSS is connected to a 400V DC grid through FPP-, and PPP-DAB converters. Comprehensive simulations for safety and power quality issues are carried out. Simulation results show that low frequency voltage harmonics can cause a high current harmonic in the battery and influence electrochemical reactions. Experimental results are carried out to validate the correctness of the simulation-based analysis.

II. Mathematical Modeling of the System

In this section, mathematical modeling of the system under study including PPPC-DAB converter and Li-ion batteries are presented.

A. Li-ion battery Dynamics

Fig. 1 (a) and (b) show the cylindrical Li-ion battery cell and its electrochemical reactions, respectively. When the battery is connected to a source, the electrons flow from the cathode to the anode through the source. This forces the Li-ions to move from the Li metal oxide ($LiCoO_2$ as an example) to the graphite anode. Therefore, the Li-ions are trapped in the layered molecular structure of the graphite up to fully charge the battery. By loading the battery, the Li-ions move back to the cathode again. This process is only possible by electrochemical reactions at the electrolyte with the anode and cathode materials. The electrochemical reactions in the battery are linked to a time constant from few ms to some seconds and mass transport is slower than seconds [22]. Propagation of current ripples with frequencies less than 1 kHz to the battery, therefore, affects the electrochemical reactions as illustrated in Fig. 1 (c). Higher frequencies are blocked by the double layer capacitor resulting from solid electrolyte interface (SEI) which resembles a low-pass filter. High frequency components mainly influence on the electromagnetic behavior of the cell.

Battery dynamics can be defined from the second order RC model, shown in Fig. 1 (b), as follows [23], [24]:

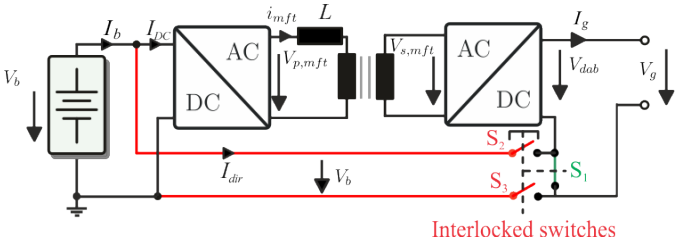

Fig. 2. BSS integration with FPP-DAB and PPP-DAB.

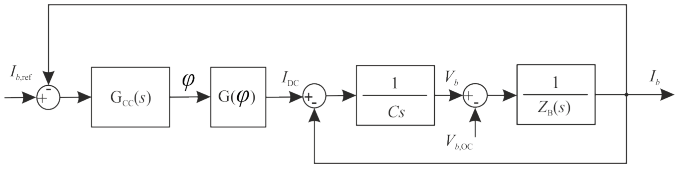

Fig. 3. Dynamic model and control loop of the FPP- and PPP-DAB converters in CC mode. The difference is the definition of $G(\varphi)$.

$$Z_B(s) = R_b + \frac{R_a}{1 + sR_aC_b} + \frac{R_c}{1 + sR_cC_c} \tag{1}$$

where R_b, R_a and R_c are the ohmic, anode and cathode SEI resistances. The double layer capacitors at anode and cathode are represented by C_a and C_c in the same order.

B. PPPC Modeling

A FPP-DAB converter can be configured to operate in PPP-DAB converter mode by pushing an interlocked switch as shown in is shown in Fig. 2. The AC/DC converters are composed of H-Bridges. In the FPP approach, the full power is processed through the converter, whereas in the PPP approach only a part of the power is processed by the converter. The rest of power is directly transferred from the input to the output.

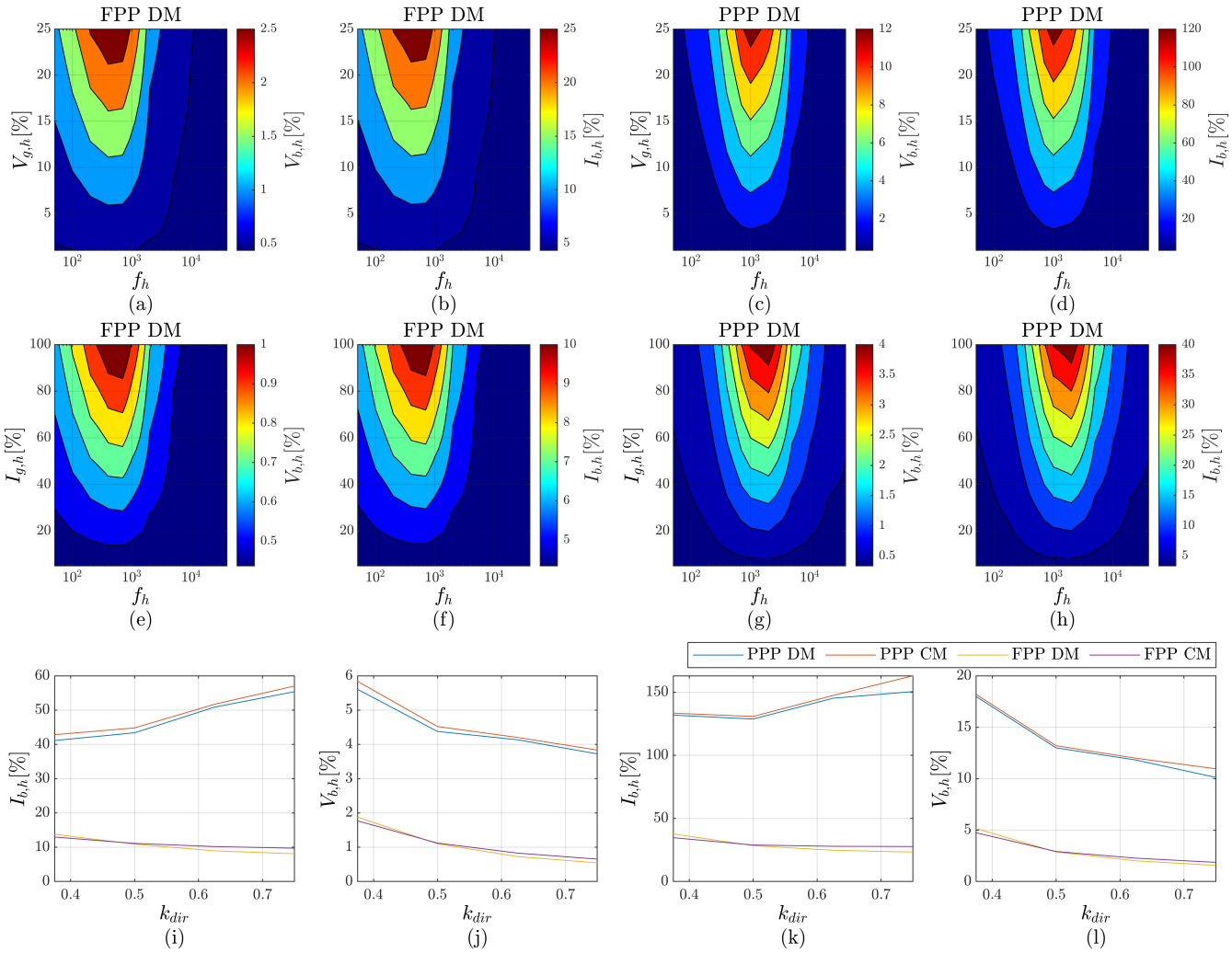

Fig. 4. Simulation results of voltage and current harmonic propagation in FPP-DAB and PPP-DAB converters: (a) the induced voltage harmonics at battery terminals integrated with FPP-DAB due to the presence of harmonics in the grid voltage, (b) the induced current harmonics at battery terminals integrated with FPP-DAB due to the presence of harmonics in the grid voltage, (c) the induced voltage harmonics at battery terminals integrated with PPP-DAB due to the presence of harmonics in the grid voltage, (d) the induced current harmonics at battery terminals integrated with PPP-DAB due to the presence of harmonics in the grid voltage, (e) the induced voltage harmonics at battery terminals integrated with FPP-DAB due to the presence of harmonics in the grid current, (f) the induced current harmonics at battery terminals integrated with FPP-DAB due to the presence of harmonics in the grid current, (g) the induced voltage harmonics at battery terminals integrated with PPP-DAB due to the presence of harmonics in the grid current, (h) the induced current harmonics at battery terminals integrated with PPP-DAB due to the presence of harmonics in the grid current, (i) the induced current harmonics for $I_{g,h} = 1.0I_{g,N}$ at different direct power transfer ratios (k_{dir}), (j) the induced voltage harmonics for $I_{g,h} = 1.0I_{g,N}$ at different k_{dir}, (k) the induced current harmonics for $V_{g,h} = 0.25V_{g,N}$ at different k_{dir}, and (l) the induced voltage harmonics for $V_{g,h} = 0.25V_{g,N}$ at different k_{dir}. In these figures' title, CM and DM show charging and discharging modes, respectively.

TABLE I
FPP-DAB AND PPP-DAB PARAMETERS.

Parameters	**FPP-DAB**	**PPP-DAB**
P_N [kW]	10	10
P_N-DAB [kW]	10	5
$V_{b,N}$ [V]/$I_{b,N}$ [A]	200/50	200/50
$V_{g,N}$ [V]/$I_{g,N}$ [A]	400/25	400/25
$V_{p,mft}$:$V_{s,mft}$	1:2	1:1
f_{sw} [kHz]	20	20

The PPP configuration in Fig. 2 can be classified to the group of Input-Parallel Output-Series (IPOS) step-up PPP converters [9]. The general operation principle is similar to conventional DAB converter. By using phase shift modulation, the active power transfer between the ports can be adjusted. Table I exemplary shows the effect for the converter design for both approaches. Considering the specifications in Table I for 50 % direct power transfer, i.e. $k_{dir} = 0.5$, the power rating of PPP-DAB can be reduced by 50 % compared to FPP-DAB.

The rectified current at the battery side of DAB converter can be directly calculated from the transferred power:

$$I_{DC} = \frac{P_{DAB}}{V_b} = \frac{V_{dab}}{\omega L}\varphi\left(1 - \frac{\varphi}{\pi}\right) \tag{2}$$

where P_{DAB} is the transferred power through the DAB, V_b

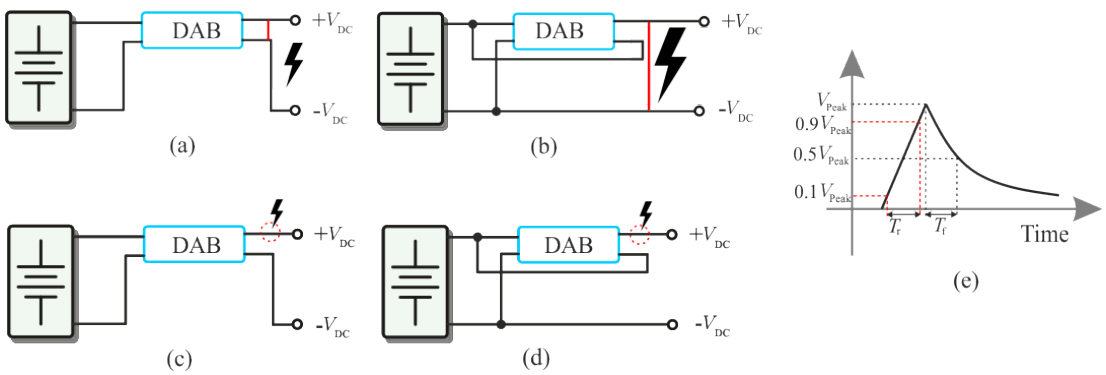

Fig. 5. Grid-side faults for FPP-DAB and PPP-DAB: (a) short-circuit fault on the FPP-DAB terminals, (b) short-circuit fault on the PPP-DAB terminals, (c) transient over-voltage fault on the FPP-DAB terminals, (d) transient over-voltage fault on the PPP-DAB terminals, and (e) transient over-voltage waveform considered in this study.

and V_{dab} the battery side and grid side voltage of the DAB converter, and φ is the phase shift between the primary and secondary H-bridges. L is the total inductance in the ac link which regulates the power flow of the DAB converter. $\omega = 2\pi f_{sw}$ and f_{sw} is the switching frequency. In the case of PPP, the total rectified current including the DAB and the direct port currents is $I_{DC}^{'} = I_{DC} + I_{dir}$. From the topology of the converter, the grid and direct port currents are equal $I_{dir} = I_g$ and it can be shown that $I_{dir} = \frac{k_{dir}}{1-k_{dir}} I_{DC}$ where $k_{dir} \in (0, 1)$. Therefore, $I_{DC}^{'}$ can be updated as follows:

$$I_{DC}^{'} = (1 + \frac{k_{dir}}{1-k_{dir}})I_{DC} = \frac{1}{1-k_{dir}} \frac{V_{dab}}{\omega L} \varphi \left(1 - \frac{\varphi}{\pi}\right) \quad (3)$$

The small-signal model is obtained by applying a perturbation, i.e. $I_b = I_{b0} + \Delta I_b$, at a given operating point I_{b0}. The small-signal model of the FPP-DAB can be extracted based on the methodology given in [25] and be extended to PPP-DAB as in [26]. The control structure of both converters is shown in Fig. 3 where G can be extracted from equations (2) and (3) for FPP- and PPP-DAB converters, respectively. It is assumed that the battery is operated at constant current (CC) mode for charging/discharging cycles.

III. Impacts on Battery

Impacts of Harmonics and short-circuits on the Li-ion battery are described in the following subsections. System parameters used for simulation studies are given in Table I. The battery pack is constructed by parallel and serial connection of 3.7V 6500mAh Li-ion cells.

A. Harmonics

The presence of current/voltage harmonics at the output of the PPP-DAB or FPP-DAB is possible due to nonlinear loads or rectification methods. Voltage/current harmonics are superimposed on the output of the PPP- and FPP-DAB converters and their propagation to the BSS side is monitored through simulations. Current controllers are designed for both FPP- and PPP-DAB converters and each k_{dir}. Voltage harmonics with f_h from 50Hz to 40 kHz and amplitudes from 1 to 25 % of the nominal grid voltage are applied and the results are shown

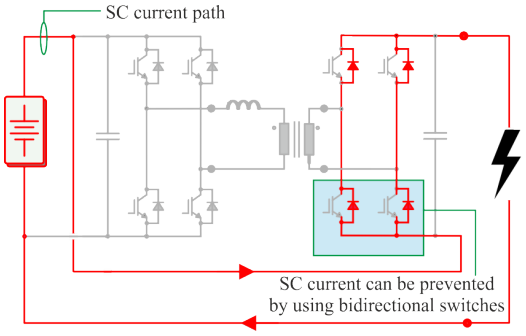

Fig. 6. Short-circuit current path in PPP-DAB converter. Fault current can be blocked by bidirectional switches in upper/lower side of the secondary H-bridges.

in Fig. 4 (a) to (d). This Figure shows that the high frequency harmonics cannot propagate to the BSS in FPP- and PPP-DAB converters. At very low frequencies, FPP- and PPP-DAB represent a similar behavior. However, PPP-DAB strongly contributes to harmonic propagation for frequencies of few hundred Hz to few kHz. For instance, voltage harmonics with $V_{g,h} = 0.25V_{g,N}$ and frequencies around f_h =1 kHz result in current harmonics $I_{b,h} = 1.2I_{b,N}$ and voltage harmonics $V_{b,h} = 0.12V_{b,N}$ in the BSS of PPP-DAB as shown in Fig. 4 (d). The harmonics in low and high frequencies are mitigated by the current controller bandwidth and the DAB converter filter, respectively. Current harmonics, $I_{g,h}$, propagate to the BSS from PPP-DAB similar to voltage harmonics at the considered frequency range as shown in Fig. 4 (g) and (h). Fig. 4 (i) to (l) show the maximum of $V_{b,h}$ and $I_{b,h}$ for k_{dir} from 0.375 to 0.75. In PPP-DAB, $V_{b,h}$ is increased and $I_{b,h}$ is decreased versus increase in k_{dir}. However, there is a big difference between the results of PPP-DAB and FPP-DAB which implies that any direct connection between the BSS and grid increases the rate of harmonic propagation. Voltage harmonics can impose high current harmonics which limit the average charging current rate increasing the heat generation more than three times for $V_{g,h} = 0.25V_{g,N}$.

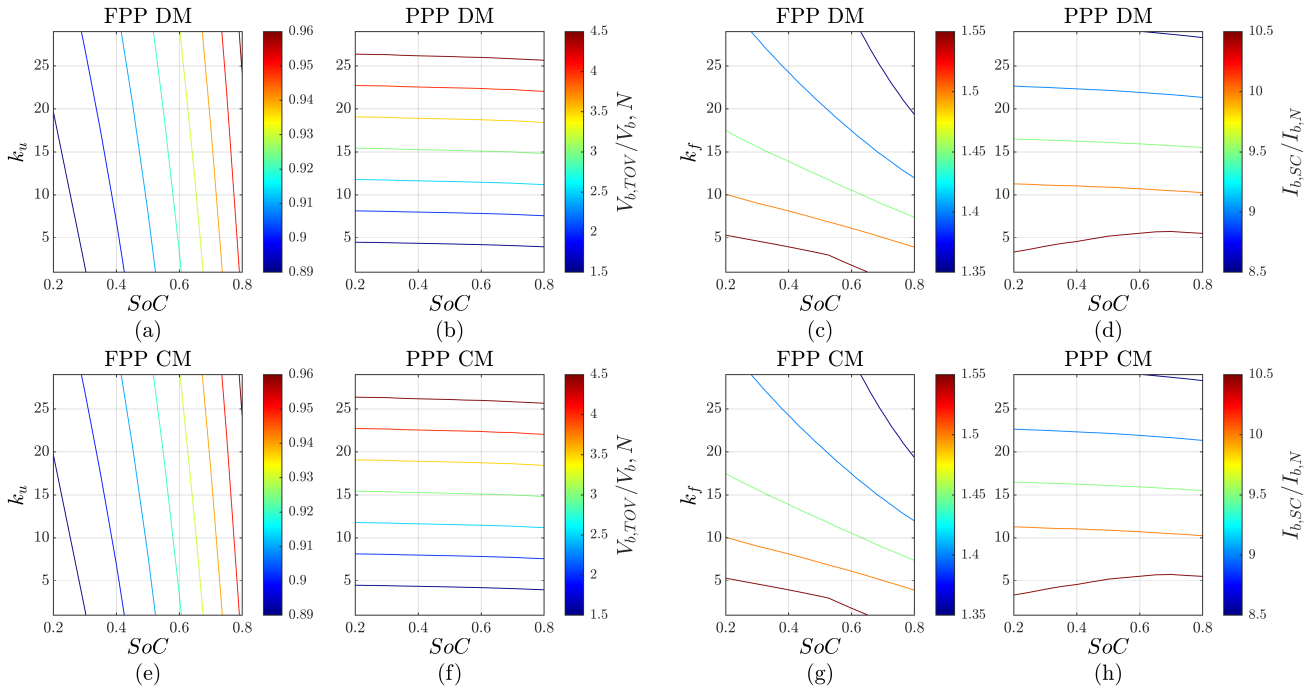

Fig. 7. Fault simulation results for FPP-DAB and PPP-DAB: (a) BSS voltage response to TOVs in FPP-DAB converter at discharging mode, (b) BSS voltage response to TOVs in PPP-DAB converter at discharging mode, (c) BSS voltage response to SCs in FPP-DAB converter at discharging mode, (d) BSS voltage response to SCs in PPP-DAB converter at charging mode (e) BSS voltage response to TOVs in FPP-DAB converter at charging mode, (f) BSS voltage response to TOVs in PPP-DAB converter at discharge mode, (g) BSS voltage response to SCs in FPP-DAB converter at charging mode, (h) BSS voltage response to SCs in PPP-DAB converter at charging mode.

B. Faults

Faults might occur due to components failure or may propagate from the grid to the devices. Fig. 5 shows SC and TOV faults on FPP-DAB and PPP-DAB converters from grid side. When the DAB impedance is in the SC path of the fault current, as in Fig. 5 (a), the SC has no impact on the BSS because the fault current is neutralized by the DAB converter itself. When the SC happens in the case of Fig. 5 (b) the DAB output voltage approaches zero. However, the anti-parallel diodes of the grid-side H-bridge connect the faulty current to the direct power flow port and short BSS terminals. Fig. 6 represents the fault current path in this situation. The source of a TOV can be a Lightning or a transient switching. Generally, the severity of lightning surge is much more higher than switching surges. Therefore, in this study the focus are TOVs as a consequence of lightning surges. A standard lightening surge waveform, shown in Fig. 5 (e), can be defined as:

$$V_{TOV} = \begin{cases} \frac{0.8V_{peak}}{T_r}t & \text{if } t < t_{peak} \\ V_{peak}\exp\left(-\frac{2}{\pi T_f}t\right) & \text{else} \end{cases} \quad (4)$$

where T_r is the rise time, T_f is the time at which the V_{peak} reduces to half after the strike. V_{peak} is the peak value of the sure voltage and t_{peak} is the time of peak voltage occurrence.

PLECS based simulations are carried out for studying the response of FPP- and PPP-DAB converters to SCs and TOVs and results are given in Fig. 7 (a) to (h). The simulated SC currents and TOVs due to faults in Fig. 5 (a) to (d) are presented. For SCs, the fault resistance is $R_f = 0.1\%Z_b k_f$ where k_f is from 1 to 30 and $Z_b = V_{g,N}^2/P_N$. Lightning surges are imposed by a 1.2/50μs lightning voltage waveform with a magnitude $V_{g,N}k_u$ where k_u is from 1 to 30. For $k_u = 30$ maximum overvoltage is around $4.5V_{b,N}$ for DM and it increases to around 5.5 for CM as in Fig. 7 (b) and (f), respectively. For $k_f = 1$ in DM and CM (SoC=0.8), the maximum SC current imposed on BSS are 10.5 and 9.5 times higher than the BSS nominal current as in Fig. 7 (d) and (h), respectively. Due to the high level of SC currents, the SC protection function of the battery management system (BMS) must be designed to avoid any damage during SC faults in PPP-DAB converters. The SoC has no effect on the voltage rise during TOVs while it has a noticeable impact on the BSS current during SCs.

IV. Experimental Verification

The BSS voltage and current response to the presence of 25% voltage harmonic at time 100ms for FPP-DAB and PPP-DAB are shown in Fig. 8 for f_h =50Hz in CM. Corresponding experiments are carried out at this frequency and are shown in Fig. 9. Fig. 9 (a) shows the DAB laboratory prototype which is configured in both FPP and PPP to verify the simulation results. Its waveforms during PPP operation are shown Fig. 9 (b). DC grid is formed by a bidirectional power supply (EA-PSB 9750-40 3U) with the ability of producing voltage/current ripples in addition to the main DC voltage. BSS is emulated by the electronic load Chroma 63804. Fig.

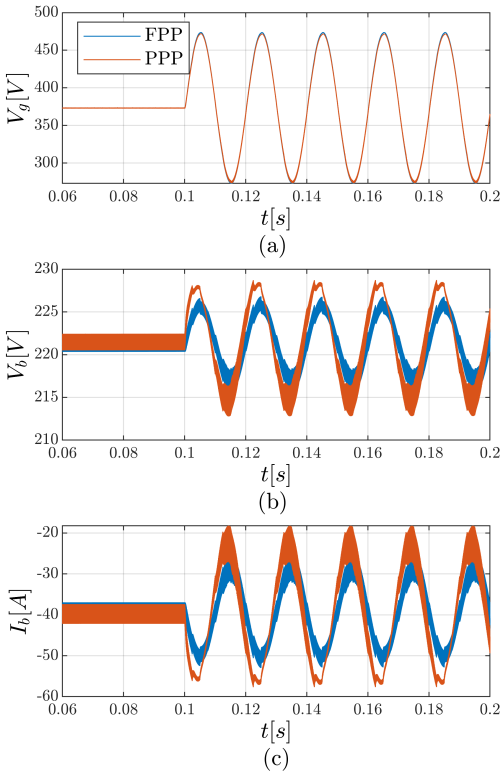

Fig. 8. Simulation of a sample waveforms due to 25 % voltage harmonic in DC grid: (a) grid voltage $\approx V_{g,N} + V_{g,h}$ as the input of the FPP-DAB and PPP-DAB converters, (b) BSS side voltage $\approx V_{b,N} + V_{b,h}$ measured at the output of the FPP-DAB and PPP-DAB converters, and (c) BSS side current $\approx I_{b,N} + I_{b,h}$ measured at the output of the FPP-DAB and PPP-DAB converters.

9 (c) and (d) illustrate the AC components of BSS (CM) and grid voltage for f_h =50Hz in FPP-DAB and PPP-DAB, respectively. For the same amount of voltage ripple in the source the measured ripple of the FPP-DAB is less than PPP-DAB. Similar results can be extracted from Fig. 4 (b), (d) and Fig. 8 (b) where voltage harmonics are shown at different frequencies. To demonstrate the frequency behaviour of the PPP-DAB converters a set of experiments are carried out. A voltage harmonic of 10 % and superimposed on the grid voltage of 100V and the propagated voltage and harmonics are measured from the battery terminals as shown in Fig. 10 (a) and (b), respectively. These results are compatible with the results from simulations, e.g. Fig. 4 (c) and (d). It can be observed that PPP-DAB converter directs the voltage and current harmonics to the battery significantly.

Remedial solutions can be considered to subside the negative impact of harmonics, SC, and TOVs on the BSSs. A configurable low-pass passive filter can be used in the output of the PPP-DAB converter to reduce the propagation of the harmonics as in [26]. The SCs and TOVs currents can be blocked by utilizing bidirectional switches instead of the low-side switches of the grid side H-bridge as highlighted in blue color in Fig. 6. Moreover, high-speed fault detection algorithm might be used to enhance the BMS performance of the battery

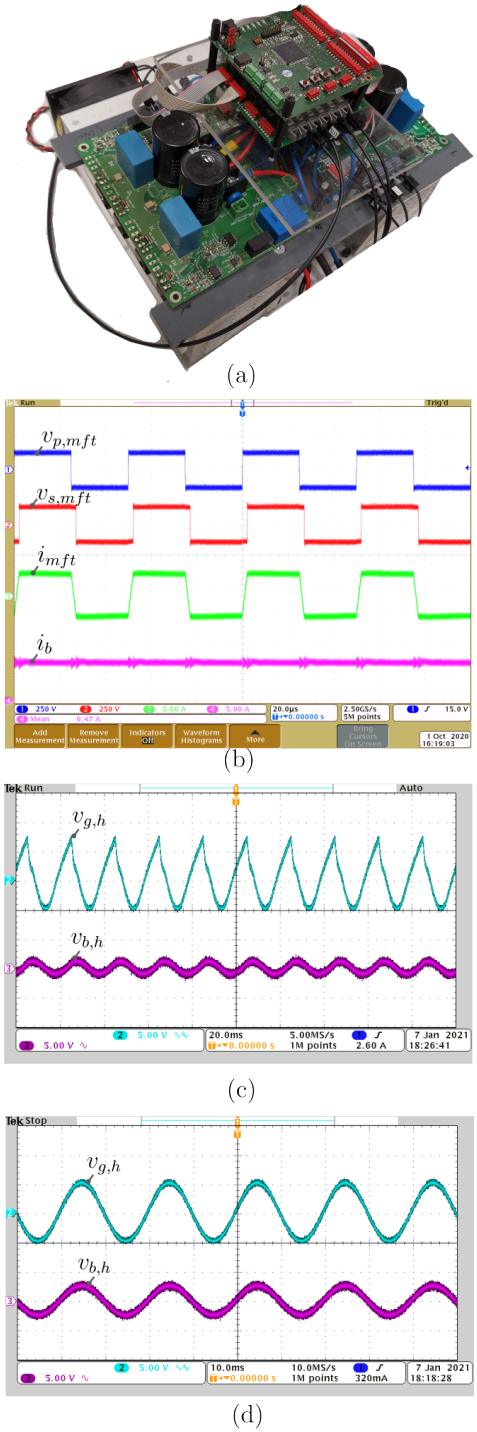

Fig. 9. Experimental results for propagation of voltage harmonics in FPP-DAB and PPP-DAB: (a) Photo of the DAB converter which is configurable in FPP-DAB and PPP-DAB, (b) Exemplary current and voltage waveforms of the PPP-DAB converter operation, (c) Applied voltage harmonic to the converter input and propagated voltage harmonic in FPP-DAB, and (d) Applied voltage harmonic to the converter input and propagated voltage harmonic in PPP-DAB.

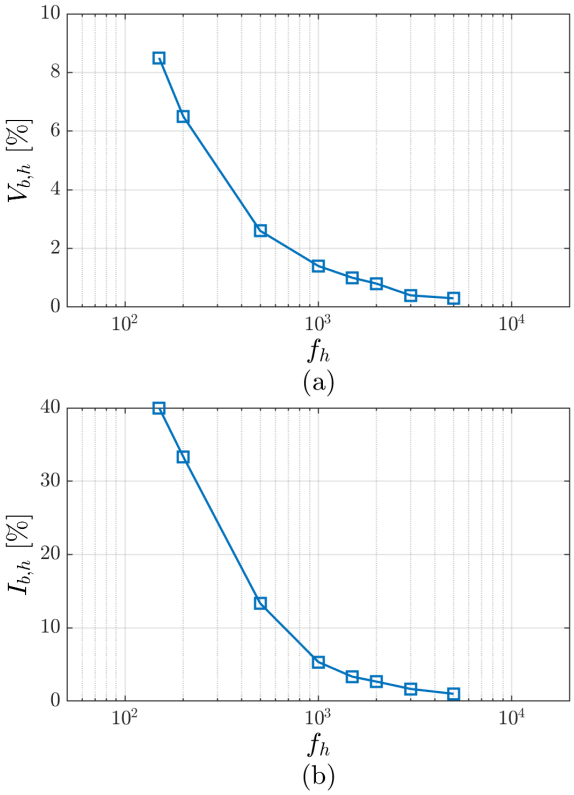

Fig. 10. Experimental results for representing the frequency behaviour of the PPP-DAB converter: (a) voltage harmonics and (b) current harmonics at the battery terminals

pack to override the propagated faults from the batteries.

V. Conclusion

Considering the recognized advantageous characteristics of PPPCs, the paper deals with the impacts of PPPCs on Li-ion batteries. To this aim, FPP-DAB and PPP-DAB are considered for comparison study. Harmonics and faults propagation to the BSS are analyzed for both topologies. Main results are highlighted as: (1) Small harmonics in the grid voltage can lead to high current harmonics in PPP-DAB integrated BSS. It reduces the effective charge current and charge time and increases the heat generation. (2) Any direct connection of batteries by the PPP-DAB significantly contribute to the harmonic and fault propagation in comparison to FPP-DAB. (3) In PPP-DAB, harmonics are mitigated by DAB and current control low-pass filters. While frequencies in the range of few hundred Hz to few kHz are not damped and can effectively influence on the electrochemical reactions of Li-ion cells, and (4) grid-side anti-parallel diodes of IGBTs in PPP-DAB conduct the faulty current to the BSS and hence the vulnerability of BSS in PPPC operation increases.

Acknowledgment

Funded by the European Union - European Regional Development Fund (EFRE), the German Federal Government and the State of Schleswig-Holstein.

References

[1] M. Stecca, L. R. Elizondo, T. B. Soeiro, P. Bauer, and P. Palensky, "A comprehensive review of the integration of battery energy storage systems into distribution networks," *IEEE Open Journal of the Industrial Electronics Society*, vol. 1, pp. 46–65, 2020.

[2] M. Kabir and D. E. Demirocak, "Degradation mechanisms in li-ion batteries: a state-of-the-art review," *International Journal of Energy Research*, vol. 41, no. 14, pp. 1963–1986, 2017.

[3] A. Abaza, S. Ferrari, H. K. Wong, C. Lyness, A. Moore, J. Weaving, M. Blanco-Martin, R. Dashwood, and R. Bhagat, "Experimental study of internal and external short circuits of commercial automotive pouch lithium-ion cells," *Journal of Energy Storage*, vol. 16, pp. 211–217, 2018.

[4] "Electric vehicle conductive charging system - Part 23: DC electric vehicle charging station (VDE 0122-2-3:2018-03)," RFC, April 2018. [Online]. Available: https://www.vde-verlag.de/standards/1100489/e-din-en-61851-23-vde-0122-2-3-2018-03.html

[5] F. Hoffmann, L. Camurca, and M. Liserre, "Modular ev fast charging station architectures based on multiphase-medium-frequency transformer," in *IECON 2018-44th Annual Conference of the IEEE Industrial Electronics Society*. IEEE, 2018, pp. 1327–1332.

[6] F. Hoffmann, J.-L. Lafrenz, M. Liserre, and N. Vazquez, "Multiwinding based semi-dual active bridge converter," in *2020 IEEE Applied Power Electronics Conference and Exposition (APEC)*. IEEE, 2020, pp. 2142–2149.

[7] G. Wang, G. Konstantinou, C. D. Townsend, J. Pou, S. Vazquez, G. D. Demetriades, and V. G. Agelidis, "A review of power electronics for grid connection of utility-scale battery energy storage systems," *IEEE Transactions on Sustainable Energy*, vol. 7, no. 4, pp. 1778–1790, 2016.

[8] K. Tytelmaier, O. Husev, O. Veligorskyi, and R. Yershov, "A review of non-isolated bidirectional dc-dc converters for energy storage systems," in *2016 II International Young Scientists Forum on Applied Physics and Engineering (YSF)*. IEEE, 2016, pp. 22–28.

[9] J. Anzola, I. Aizpuru, A. A. Romero, A. A. Loiti, R. Lopez-Erauskin, J. S. Artal-Sevil, and C. Bernal, "Review of architectures based on partial power processing for dc-dc applications," *IEEE Access*, vol. 8, pp. 103 405–103 418, 2020.

[10] D. Ouyang, M. Chen, J. Liu, R. Wei, J. Weng, and J. Wang, "Investigation of a commercial lithium-ion battery under overcharge/over-discharge failure conditions," *RSC advances*, vol. 8, no. 58, pp. 33 414–33 424, 2018.

[11] Q. Yuan, F. Zhao, W. Wang, Y. Zhao, Z. Liang, and D. Yan, "Overcharge failure investigation of lithium-ion batteries," *Electrochimica Acta*, vol. 178, pp. 682–688, 2015.

[12] W. Mei, L. Zhang, J. Sun, and Q. Wang, "Experimental and numerical methods to investigate the overcharge caused lithium plating for lithium ion battery," *Energy Storage Materials*, vol. 32, pp. 91–104, 2020.

[13] A. Sidhu, A. Izadian, and S. Anwar, "Adaptive nonlinear model-based fault diagnosis of li-ion batteries," *IEEE Transactions on Industrial Electronics*, vol. 62, no. 2, pp. 1002–1011, 2014.

[14] C. J. Orendorff, E. P. Roth, and G. Nagasubramanian, "Experimental triggers for internal short circuits in lithium-ion cells," *Journal of Power Sources*, vol. 196, no. 15, pp. 6554–6558, 2011.

[15] X. Lai, W. Yi, X. Kong, X. Han, L. Zhou, T. Sun, and Y. Zheng, "Online detection of early stage internal short circuits in series-connected lithium-ion battery packs based on state-of-charge correlation," *Journal of Energy Storage*, vol. 30, p. 101514, 2020.

[16] V. Müller, R.-G. Scurtu, M. Memm, M. A. Danzer, and M. Wohlfahrt-Mehrens, "Study of the influence of mechanical pressure on the performance and aging of lithium-ion battery cells," *Journal of Power Sources*, vol. 440, p. 227148, 2019.

[17] B. Liu, Y. Jia, C. Yuan, L. Wang, X. Gao, S. Yin, and J. Xu, "Safety issues and mechanisms of lithium-ion battery cell upon mechanical abusive loading: A review," *Energy Storage Materials*, vol. 24, pp. 85–112, 2020.

[18] J. Lamb and C. J. Orendorff, "Evaluation of mechanical abuse techniques in lithium ion batteries," *Journal of Power Sources*, vol. 247, pp. 189–196, 2014.

[19] A. Bessman, R. Soares, S. Vadivelu, O. Wallmark, P. Svens, H. Ekström, and G. Lindbergh, "Challenging sinusoidal ripple-current charging of lithium-ion batteries," *IEEE Transactions on Industrial Electronics*, vol. 65, no. 6, pp. 4750–4757, 2017.

[20] M. J. Brand, M. H. Hofmann, S. S. Schuster, P. Keil, and A. Jossen, "The influence of current ripples on the lifetime of lithium-ion batteries," *IEEE Transactions on Vehicular Technology*, vol. 67, no. 11, pp. 10 438–10 445, 2018.

[21] R. Xiong, R. Yang, Z. Chen, W. Shen, and F. Sun, "Online fault diagnosis of external short circuit for lithium-ion battery pack," *IEEE Transactions on Industrial Electronics*, vol. 67, no. 2, pp. 1081–1091, 2019.

[22] A. Jossen, "Fundamentals of battery dynamics," *Journal of power sources*, vol. 154, no. 2, pp. 530–538, 2006.

[23] S.-Y. Cho, I.-O. Lee, J.-I. Baek, and G.-W. Moon, "Battery impedance analysis considering dc component in sinusoidal ripple-current charging," *IEEE Transactions on Industrial Electronics*, vol. 63, no. 3, pp. 1561–1573, 2016.

[24] M. Chen and G. Rincon-Mora, "Accurate electrical battery model capable of predicting runtime and i-v performance," *IEEE Transactions on Energy Conversion*, vol. 21, no. 2, pp. 504–511, 2006.

[25] V. Vlatkovic, J. A. Sabate, R. B. Ridley, F. C. Lee, and B. H. Cho, "Small-signal analysis of the phase-shifted pwm converter," *IEEE Transactions on power Electronics*, vol. 7, no. 1, pp. 128–135, 1992.

[26] V. M. Iyer, S. Gulur, G. Gohil, and S. Bhattacharya, "An approach towards extreme fast charging station power delivery for electric vehicles with partial power processing," *IEEE Transactions on Industrial Electronics*, vol. 67, no. 10, pp. 8076–8087, 2020.